Folding Properties of an Annexin I Domain: a $^{1}H-^{15}N$ NMR and CD Study

Françoise Cordier-Ochsenbein,[‡] Raphaël Guerois,[‡] Françoise Baleux,[§] Tam Huynh-Dinh,[§] Alain Chaffotte,[∥] Jean-Michel Neumann,[‡] and Alain Sanson*,[⊥]

Département de Biologie Cellulaire et Moléculaire, Section de Biophysique des Protéines et des Membranes, URA CNRS 2096, CEA Saclay, 91191 Gif-sur-Yvette Cedex, France, and Unité de Chimie Organique, URA CNRS 487, Institut Pasteur, and Unité de Biochimie Cellulaire, URA CNRS 1129, Institut Pasteur, 28 rue du Dr Roux, 75724 Paris Cedex 15, France

Received March 28, 1996; Revised Manuscript Received June 6, 1996[⊗]

ABSTRACT: The annexin fold consists of four 70-residue domains with markedly homologous sequences and nearly identical structures. Each domain contains five helices designated A to E. Domain 2 of annexin I was obtained by chemical synthesis including ten specifically labeled residues and studied by $^{1}H-^{15}N$ NMR and circular dichroism (CD). In pure aqueous solution this annexin domain presents, at most, 25% of residual helix secondary structure compared to 75%−85% for the native helix content and thus does not constitute an autonomous folding unit. Dodecylphosphocholine (DPC) micelles were used to provide the annexin domain with non-specific hydrophobic interactions. The structuring effect of micelles was thoroughly investigated by CD and $^{1}H-^{15}N$ NMR. Most, but not all, of the native helix secondary structure was recovered at DPC saturation. NMR data made it possible to determine the intrinsic helix propensity hierarchy of the different helix segments of the domain: A ∼ B ∼ E > C, D. This hierarchy is remarkably well correlated with the location of the helices in the native protein since A, B, and E helices are those in contact with the remaining parts of the protein. This result tends to support the view that, for large proteins like annexins (35 kDa), high intrinsic secondary structure propensities, at least helix propensity, in selected protein segments is necessary for a correct folding process. As a consequence this also indicates that important information concerning the folding pathway is encoded in the protein sequence.

One of the most important issues in the field of protein folding is the characterization of the successive intermediate states that bring an unfolded protein to a compact state which has the capability of allowing the final folding step to take place. Ultimately, the task is to elucidate the link existing between this ensemble of sequential early folding steps and the protein sequence or, more realistically, ensemble of homologous sequences. A great deal of progress has been made in the last few years in the description and understanding of the folding of small proteins (Dobson, 1994; Dobson et al., 1994; Fersht, 1995; Itzaki et al., 1995). Larger proteins and multidomain proteins are more complicated, and the dissection, at the molecular level, of their folding pathway—or pathways—is still largely in progress in several laboratories.

For multidomain proteins, experimental assessments of the folding propensities are required not only among the different building blocks which may be defined as domains or modules but also within their identified structural subsets. In other words we need to establish the hierarchy in the folding propensities underlying the ensemble of parallel and sequential events which construct the efficient and robust folding pathway of proteins.

In this regard, our protein of interest, a protein of the annexin family (Moss, 1992), exhibits interesting structural aspects. The annexin fold consists of four building blocks of ∼70 residues, called domains D1 to D4, which have markedly homologous sequences and nearly identical structures (Bewley et al., 1993; Concha et al., 1993; Huber et al. 1990a, 1992; Weng et al., 1993). The four domains are arranged in an almost planar, circular configuration which brings D4 into contact with D1. This arrangement leaves a rather hydrophilic channel in the center of the protein. In addition, the domains are assembled into two modules, (D1+D4) and (D2+D3). The internal structure of each domain is formed by five helix segments organized into a right-handed superhelix (A−loop−B)−C−(D−E). For most of the annexins studied so far (Favier-Perron et al., 1996; Huber et al., 1990b; Lewit Bentley et al., 1994; Sopkova et al., 1993, 1994; Weng et al., 1993), the domains harbor a characteristic calcium binding site in the loop joining the A and B helices. An acidic residue at the end of the D helix completes the site. Calcium ions participate in the functional binding of annexin to membranes. Annexin's philogeny indicates that the annexin structure results from gene duplication during evolution and originates from a small, domain-sized, ancestral protein (Barton et al., 1991; Morgan & Fernandez, 1995).

Our aim in studying the annexin family is to determine the intrinsic folding propensities at the level of the detail within secondary structure elements and at the level of the domain and module. It is important to determine these propensities, which are believed to correlate with the folding pathway during the first folding period (de Prat Gay et al., 1995; Dobson, 1994; Dobson et al., 1994, Peng & Kim, 1994; Pintar et al., 1994; Smith et al., 1994; Wu et al., 1994; Yang et al., 1995), given the presently available theories or approaches for the folding process [see for instance Baldwin (1995), Dill et al. (1995), Fersht (1995), and Nishii et al. (1994) and references therein]. Annexins have an additional

* FAX: +33 1 69 08 81 39. Phone: +33 1 69 08 28 63.
[‡] CEA Saclay.
[§] Unité de Chimie Organique, Institut Pasteur.
[∥] Unité de Biochimie Cellulaire, Institut Pasteur.
[⊥] Also from Université P. et M. Curie, 9 Quai Saint-Bernard, Bât. C, 75005 Paris, France.
[⊗] Abstract published in *Advance ACS Abstracts,* August 1, 1996.

S0006-2960(96)00747-7 CCC: $12.00

interest because of the relatively high degree of internal symmetry in their native structure. Alteration of the symmetry in the amino acid sequence may reflect, apart the normal degeneracy of the structure−sequence code and some functional aspects, a modulation of the folding propensities which may in turn reflect an optimization of the folding process, particularly regarding a possible sequentiality in the *in vivo* folding process.

In this paper, we focus on domain 2 of annexin I, which was obtained by chemical synthesis and has the following sequence:

AQFDADE***L***RA$_{10}$AMK***GLG***TDED$_{20}$T***L***IEILASRT$_{30}$-NKEI

RDINR***V***$_{40}$YREELKRDL***A***$_{50}$KDITS***D***TS***G***D$_{60}$-FRNA***L***LSLAK$_{70}$

The ten residues in italics were ^{15}N-labeled for NMR studies. This fragment was studied by circular dichroism and by NMR. Both techniques clearly showed that the domain was poorly folded in pure aqueous solution although the residual helix structure is far from negligible. The fragment was then studied in aqueous solution containing various amounts of perdeuterated dodecylphosphocholine (DPC),[1] which forms micelles. The goal here is to observe the onset of secondary structures due to nonspecific hydrophobic interactions which are expected to occur at the approach to the transition state during the first period of the folding. We were able to analyze the data in terms of helical propensities. Remarkably, this hierarchy is directly related to the helix organization in the native structure. If we except two persistent nonnative local structures, the full native secondary structure was recovered at DPC saturation, which was shown to correspond to one domain for one micelle. Nevertheless, the overall structure obtained does not correspond to the native compact state as judged by the mobility of several side chains and the inability to specifically bind calcium ions.

MATERIALS AND METHODS

Synthesis of annexin I domain 2. The peptide was synthesized by the Merrifield solid-phase method (Merrifield, 1963) on an Applied Biosystems 430 A synthesizer using 0.5 mmol of Boc-Lys(2-Cl-Z)-Pam resin. Stepwise elongation of the peptide chain was done using the standard coupling−capping protocols. Boc[^{15}N]Asp(OBzl)OH, [^{15}N−^{13}C]Gly, [^{15}N]Ala, [^{15}N]Leu, and [^{15}N]Val were from EurisoTop, France. The Boc group was introduced via di-*tert*-butyldicarbonate (Moroder et al., 1976).

To optimize the synthesis of this long sequence (70 amino acids) the first 23 residues were all double-coupled and at this point, the peptide-resin was split in two parts, and the synthesis was continued with 1.2 g, yielding 2.4 g of the 70 amino acid peptide−resin (yield, 67%).

Peptide resin (0.8 g) was subjected to low−high HF cleavage (Tam & Heath, 1983). Part of the crude peptide (354 mg) was prepurified on Bio-Gel P-10 using 0.1 M AcOH as eluent. The peptide (190 mg) was then purified by MPLC (medium-pressure liquid chromatography) on an HD-SIL 15−25 ptm C18 100 Å preparative column, using a 30%−60% linear gradient of acetonitrile in 0.08% aqueous TFA (pH 2) for 60 min at 25 mL/min flow rate. After amino acid analysis, the MPLC fraction (37 mg) having the required amino acid composition was purified on a Nucleosil 5 mm C18 300 Å semipreparative column, using a 20%−70% linear gradient of the same eluents as above, at 6 mL/min flow rate. The final purity of the peptide was checked on a Nucleosil 5 mm C18 300 Å analytical column, using a 30%−60% linear gradient of the same eluents as above for 20 min, at 1 mL/min flow rate (t_R = 14.65 min) and a 5%−70% linear gradient of acetonitrile in 10 mM TEAP pH 7 for 20 min (t_R = 10.46 min). Yield: 10 mg.

The purities of the final peptide in these two different pH eluent conditions were respectively 83% and 95%. The observed difference could be due to the peptide having different conformations at pH 7 (ionization states) giving closely related molecules detected by analytical reverse phase HPLC, conformations not present at pH 2. Positive ion electrospray ionization mass spectra: 7911.50 Da (expected: 7912.04 Da).

CD Spectra. CD spectra were recorded on a Jobin-Yvon (Longjumeau, France) CD6 spectrodichrograph, using a 0.1 mm path length cell. The temperature was kept at 293 K, and the scanned wavelength region was 192−255 nm. The spectral bandwidth was 2 nm, and the wavelength increment and the accumulation time were 0.2 nm and 1 s per step, respectively. Each spectrum resulted from averaging five successive individual spectra, and the spectrum of the solvent alone was recorded under identical conditions and subtracted. The presence of DPC micelles did not modify the solvent spectrum. The secondary structure content was estimated according to Yang et al. (1986), and the peptide concentration determined by amino acid analysis was 0.72 mg/mL. The solvent used was the same as for NMR studies: 35 mM Tris buffer, 200 mM NaCl, pH 7. CD spectra were recorded at DPC concentrations varying from 0.5 to 10 mM

CMC Measurement. ANS (8-anilino-1-naphthalenesulfonic acid) fluorescence was used to determine the cmc of DPC in the absence and presence of the peptide (Ortner et al., 1979). Fluorescence intensity, using activation and emission wavelengths of 370 nm and 490 nm, respectively, in a solution of 4 μM ANS in 35 mM Tris buffer, 200 mM NaCl, pH 7, was measured in the absence or presence of 0.6 mg of annexin I domain 2/mL. ANS fluorescence was experimentally measured for increasing amounts of DPC (data not shown). Without annexin I domain 2, the DPC cmc was 1.1 mM and was reduced to 0.9 mM in the presence of the peptide. The value without peptide is identical to that obtained by Stafford et al. (1989) using ^{31}P NMR.

Polyacrylamide Gel Electrophoresis. Protein samples were electrophoresed under denaturing (0.4% SDS and boiled) and non-denaturing conditions. In both cases, 20% acrylamide gel was used. Protein gels were fixed using 2.5% glutaraldehyde and stained with Coomassie Blue (Bollag & Edelstein, 1995).

[1] Abbreviations: ANS, 8-anilino-1-naphthalenesulfonic acid; CD, circular dichroism; cmc, critical micelle concentration; DPC, dodecylphosphocholine; COSY, correlated spectroscopy; CPMG, Carr−Purcell−Meiboom−Gill; EDTA, ethylenediaminetetraacetic acid; HMQC, heteronuclear multiple-quantum correlation; HSQC, heteronuclear single-quantum correlation; NMR, nuclear magnetic resonance; NOE, nuclear Overhauser effect; NOESY, nuclear Overhauser enhancement spectroscopy; R_2, transverse relaxation rate; SDS sodium dodecyl sulfate; T_2, transverse relaxation time; TFE, trifluoroethanol; TOCSY, total correlated spectroscopy.

NMR Experiments

^{1}H and ^{15}N NMR Spectroscopy. 8 mg of free peptide was dissolved in 0.4 mL of perdeuterated Tris buffer containing 0.1 mM EDTA, 200 mM NaCl, and 50 μL of D_2O, and the pH was adjusted to 7.0. Standard 600 MHz two-dimensional phase sensitive experiments (COSY, TOCSY, and NOESY; Markley, 1989; Wüthrich, 1986) were performed on a Bruker AMX 600 spectrometer. Mixing times of 80 and 160 ms were used for TOCSY and NOESY experiments, respectively. Heteronuclear HSQC (Lerner & Bax, 1986), gradient-enhanced HSQC (Grzesiek & Bax, 1993), HMQC-COSY (Gronenborn et al., 1989), and ^{15}N T_2 measurement (Kay et al., 1989) spectra were recorded on a Bruker AMX 500 equipped with a gradient accessory. A GARP ^{15}N-decoupling sequence (Shaka et al., 1985) was used in several homonuclear experiments and in all heteronuclear experiments. Spectra were recorded at different temperatures, varying from 278 to 313 K, and at different deuterated dodecylphosphocholine (DPC) micelle concentrations. In general, COSY, TOCSY, NOESY, and HMQC-COSY spectra were acquired with a recycling delay of 1 s and 400 increments of 2K data points and HSQC spectra were acquired with 256 increments of 2K data points. For ^{15}N T_2 experiments, a recycling delay of 3 s was used. Shifted sine-bell and shifted squared sine-bell functions were used for apodization. Data were processed using UXNMR software (Bruker).

^{31}P NMR Relaxation Studies. ^{31}P NMR spectra were recorded for a 35 mM Tris buffer, 200 mM NaCl, 0.1 mM EDTA, pH 7, sample containing 9 mg of DPC. Annexin I domain 2 was added at a molar ratio of 1/50, corresponding to the plateau region of the titration curve. The transverse ^{31}P relaxation rate (R_2) of DPC micelles was measured at 202 MHz on a Bruker AMX 500 spectrometer in the presence and absence of peptide. A standard Carr−Purcell−Meiboom−Gill (CPMG) sequence was used with a recycling delay of 10 s and a refocusing delay of 2 ms. No ^{1}H−^{31}P NOE was detected, thus confirming that the ^{31}P relaxation is governed by the chemical shift anisotropy at 202 MHz.

RESULTS

CD and NMR Data for the Annexin 1 Domain 2 Solubilized in Aqueous Solution

Ten ^{15}N-labeled amino acids were incorporated in the synthesized domain. Their corresponding locations in the crystallographic structure (Weng et al., 1993) are shown in Figure 1. L8, L22, V40, A50, and L65 are respectively within each of the five native helices (A−E), G59 is at the hinge between the D and E helices, and the other labeled amino acids are involved in the calcium site, G14-L15-G16 in the loop between the A and B helices and D56 as the bidentate chelator.

A first set of NMR experiments was performed on the domain solubilized in pure aqueous solution, in which the very weak spectral dispersion of the amide proton resonances (1.1 ppm) showed that the peptide is poorly folded. Although the high degeneracy of the NH signals precluded the resonance assignment of the domain, the amide ^{1}H and ^{15}N signals of the labeled residues could be assigned, by continuity, from the HSQC spectrum evolution upon addition of DPC micelles (see the following main section and Figure 11) after assignment of the resonances at high DPC content. The corresponding Hα resonances were then assigned using a HMQC-COSY spectrum. The ΔHα difference $\delta H\alpha_{obs} - \delta H\alpha_{coil}$, where the $\delta H\alpha_{obs}$ is the experimental chemical shift and $\delta H\alpha_{coil}$ is the corresponding coil value given by Merutka et al. (1995), measured for each labeled residue is shown in Figure 2. The ΔHα of residues in the segments spanning the native A, B, C, and E helices exhibit negative values (between −0.1 and −0.2 ppm) characterizing helix structures. However, the largest ΔHα values (A and B segments) are far from that expected for stable helices (about -0.4 ppm) (Chupin et al., 1995; Jimenez et al., 1994; Munoz & Serrano, 1995; Munoz et al., 1995; Papavoine et al., 1994). The ΔHα of the G14-L15-G16 residues (native loop) and those of A50 (D helix) and G59 (E helix) are quite weak, whereas that of D56 (D helix) is positive.

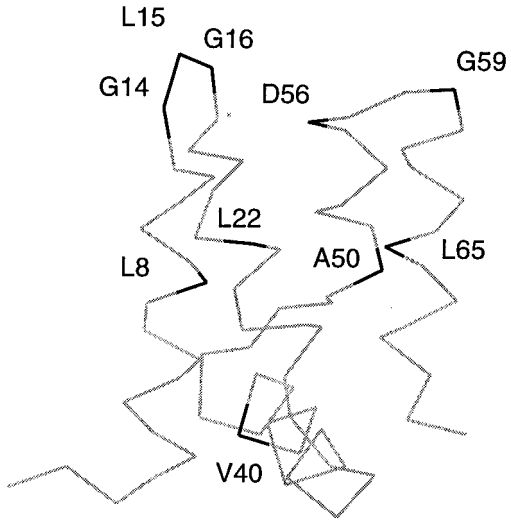

FIGURE 1: Native structure of annexin I domain 2. The ten labeled amino acids incorporated in the synthesized domain are indicated by the corresponding residue number.

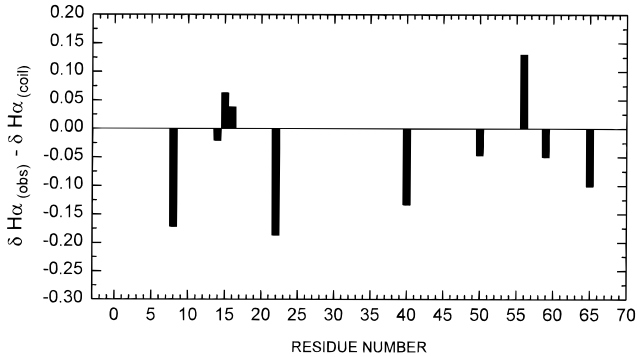

FIGURE 2: Hα chemical shift difference, $\Delta H\alpha = \delta H\alpha_{obs} - \delta H\alpha_{coil}$, for the ten labeled residues in aqueous solution (pH = 7, 303 K) assigned using a HMQC-COSY spectrum.

The helix content of the domain in the annexin native structure is in the range 75%-85% depending on whether the transition residues at the helices' ends are counted or not. Deconvolution of the far-UV CD spectrum of the isolated domain in aqueous solution, using the Yang reference, gave a secondary structure content of, at most, 25% α helix, 75% coil, and no β structure. This helix content is quite far from the native content. Therefore the isolated domain does not constitute an autonomous folding unit and obviously needs the long-range interactions involving residues of the other domains. Examination of the annexin

native structure shows that domain 2 and domain 3 interact *via* a hydrophobic interface which constitutes the ensemble of long-ranged hydrophobic interactions necessary for the initiation and stabilization of the tertiary fold of domains 2 and 3. In this context, micelles were added to provide the annexin domain with such hydrophobic interactions, actually, nonspecific hydrophobic interactions which are supposed to mimic the interactions present at certain steps of the initial collapse during the folding process. This hypothesis is supported by previous NMR studies of a domain 2 fragment, spanning the A helix−loop−B helix motif (Macquaire et al., 1993), showing that addition of DPC micelles to the peptide solution not only strongly stabilized both helices but also induced a tertiary-like structure.

CD and NMR Data for the Annexin 1 Domain 2 Solubilized in Aqueous DPC Micellar Solution

CD Data. As expected, addition of micelles led to a considerable increase in the helix content (Figure 10). Above a DPC/peptide ratio of 6, the ellipticity remained constant. The determination of the helix content for a protein in a micelle environment is not straightforward (Fasman, 1995), and this content tends to be overestimated by the Yang method. For the domain 2 in DPC micelles, a 65%−75% range is a reasonable estimate of the helix content, and thus, the native helix content, is not recovered.

Assignment of the ^{15}N and ^{1}H Resonances. The assignment of the ^{15}N resonances was generally straightforward by using proton NOESY spectra on one hand, recorded with or without ^{15}N decoupling, which allows the immediate locating of the labeled residues, and HMQC-NOESY spectra on the other hand. The three consecutive ^{15}N-labeled residues G14-L15-G16 were easily assigned because of the characteristic ^{15}N chemical shift of glycine residues and the presence of the sequential αN(i,i+1) cross-peaks observed in the NOESY spectra. Consequently, the third ^{15}N-labeled glycine residue, G59, was *de facto* assigned. Residue D56 is the sole ^{15}N-labeled aspartate residue of the peptide and can be easily assigned because of its characteristic spin system. Residue V40 is the sole valine residue of the peptide and was immediately identified by its typical γ or γ' resonance at 1.01 ppm confirmed by the sequential γV40-Y41 NOE contact. Residue A50 is the sole ^{15}N-labeled alanine residue of the peptide and was immediately identified by its β resonance. The remaining ^{15}N-labeled leucine residues L8, L22, and L65 were assigned as follows. Residue L22 was straightforwardly assigned by the sequential γT21-HNL22 arising from the well-separated γT21 protons at 1.24 ppm. The two remaining leucine residues have approximately the same amide proton chemical shift, but the L65 residue can be identified by the medium-distance δL65-F61 NOE contact arising from the particularly high-field-shifted δL65 resonance at 0.78 ppm. Returning to the HMQC-NOESY spectrum, the intraresidue δ65-HN65 contact allowed the assignment of the L65 ^{15}N resonance and deductively that of L8.

At high DPC concentration (150 mM), the NH spectral range was considerably larger than that observed in pure aqueous solution (1.7 ppm against 1.1 ppm for the pure aqueous solution). However, due to the size of the domain−micelle complex (20−25 kDa) and the well-known weak spectral dispersion of the Hα signals for helix structure, only a partial assignment was possible. With the additional help of the ^{15}N-labeled residues as starting points, the resonance assignment of 52 residues, including the ^{15}N-labeled residues, was achieved using homonuclear TOCSY and NOESY spectra as well as heteronuclear spectra (HSQC, HMQC-COSY) recorded at different temperatures between 303 and 323 K. Typical NOESY spectra are shown in Figure 3a and b, together with sample of attribution pathways concerning the E helix resonances. In addition, from the assignment of the ^{1}H and ^{15}N amide signals of the labeled residues at 50 mM DPC, we were able to assign all the HSQC spectra recorded for intermediate DPC concentrations down to 0 mM DPC (Figure 4), following the resonance along the titration.

Hα Chemical Shift Analysis. For the reasons already mentioned, the nonambiguous medium-range ^{1}H−^{1}H NOEs were too scarce to allow a relevant conformational analysis. Fortunately, recent statistical studies assessed the Hα chemical shift as a reliable index of secondary structure, especially in the case of helices, and the ΔHα profiles ($\Delta H\alpha = \delta H\alpha_{obs} - \delta H\alpha_{coil}$) are now currently used as a conformational index in NMR studies of peptides and proteins (Wishart & Sykes, 1994; Wishart et al., 1991a,b, 1992). The ΔHα values measured for all the assigned residues of the annexin domain are shown in Figure 5. For the three segments spanning the A, B, and E native helices, the corresponding ΔHα profiles obtained for all assigned residues are consistent with stable amphipathic helices: large negative ΔHα values (up to −0.55 ppm) and characteristic (i,i+4) pseudo-oscillations (Jimenez et al., 1992). Using the one-digit index of Wishart et al. (1992), the extention of the helices, as determined from the ΔHα, is indicated as grey bars for comparison with the crystallographic data which are indicated as black bars. For the A helix, the large positive ΔHα value of D4 clearly indicates the presence of a non-native structure at the N terminal end. The existence of a non-native D_4ADE_7 capping box structure has recently been demonstrated for the N-terminal 21-residue peptide spanning the A helix of the annexin I domain 2 and thoroughly analyzed (Odaert et al., 1995). In the segment spanning the native C helix, negative ΔHα values were also found, indicating the presence of a helical structure. However, the (i,i+4) periodicity of the ΔHα profile is poorly defined, which indicates that this helix is probably not fully stabilized at DPC saturation. For the segment corresponding to the native D helix, there are not enough assigned Hα signals to allow a clear-cut conformational description. However, the large positive ΔHα value of D56, the penultimate residue of D helix, strongly suggests the presence of a non-native structure in the C-terminal. Lastly, the ΔHα profile is consistent with a well-defined loop between the A and B helices close to the native one. In particular, on addition of DPC micelles, the Hα and Hα′ signals of both G14 and G16 residues became markedly magnetically nonequivalent with an average ΔHα value close to zero as already observed for the fragment spanning the A helix−loop−B helix motif (Macquaire et al., 1993). The result of the ΔHα analysis is further supported by several NOE data, namely, (i) the presence of ∼36 nonambiguous NN(i,i+1) cross-peaks, some of which are rather intense, mainly involving residues located in the A, B, and E helices (Figure 3b); (ii) a few nonambiguous medium-range NOEs such as the αN(i,i+3) M12-L15, I25-S28, R62-L65, L66-A69, and S67-K70.

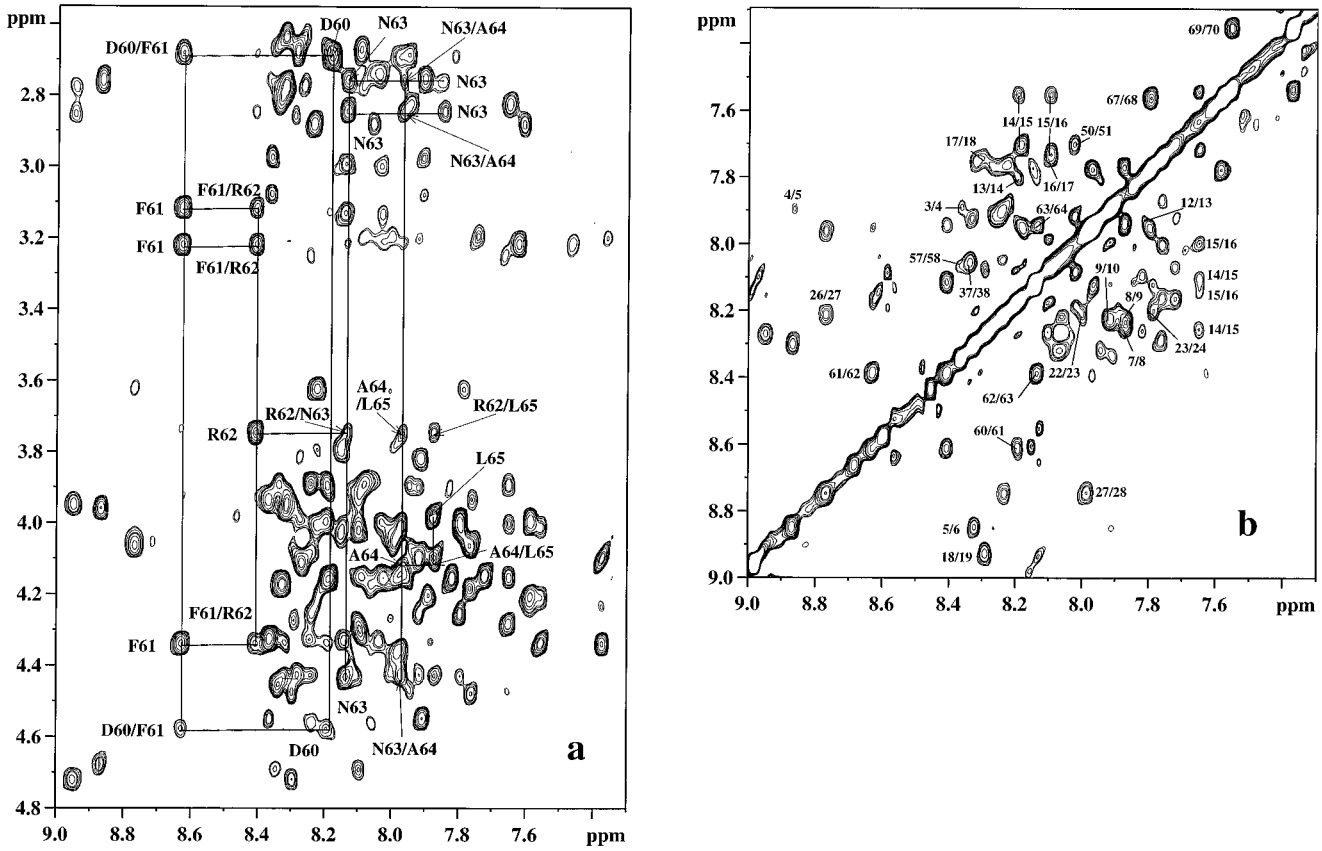

FIGURE 3: The α/β-HN region (a) and the amide region (b) of the 600 MHz NOESY spectrum of the domain 2 solubilized in 140 mM DPC (pH = 7, 313 K). A sample of assignment pathways for residues in the E helix is indicated.

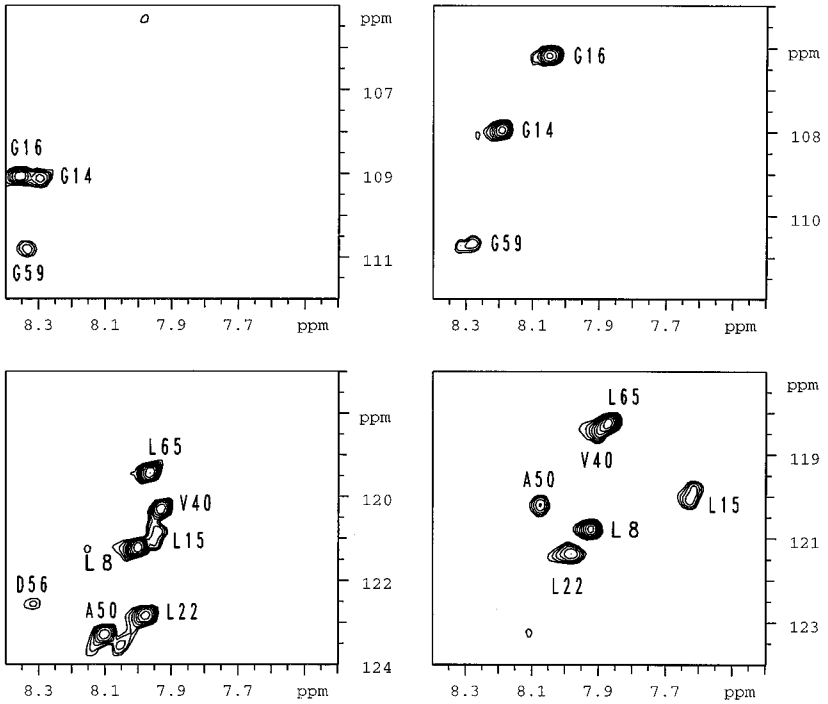

FIGURE 4: 500 MHz $^1H-^{15}N$ HSQC spectrum of annexin I domain 2 in aqueous solution (pH = 7, 303 K) (left), and with 50 mM DPC (right). Cross-peaks are labeled with the residue numbers.

Aromatic Side-Chain Interactions. Aromatic side chains can be useful reporters for testing the compactness of the domain within a micelle. Figure 6 shows the aromatic region of the NOESY spectrum of the domain solubilized in micelles at 313 K. The F3 chain exhibits approximately the same contacts as those observed for the isolated A helix fragment in micelles (unpublished data) and, in particular, the F3-L8 contact characteristic of the hydrophobic cluster associated with the non-native capping box. Y41 also presents a number of NOE contacts, which could not be completely attributed although some of them can be guessed since they correspond to possible Arg and Glu resonances which are residues close to Y41 in the sequence (Figure 6). F61 aromatic protons present relatively high-intensity NOE

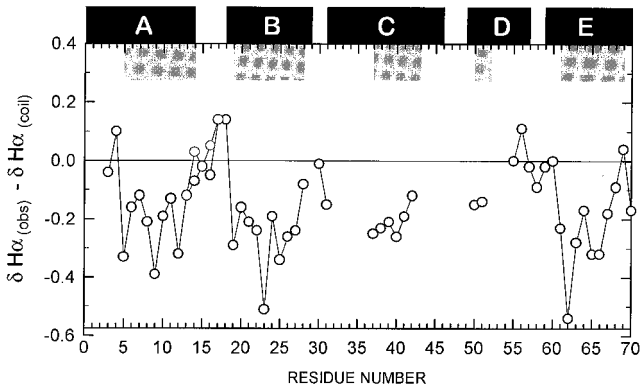

FIGURE 5: Hα chemical shift difference, $\Delta H\alpha = \delta H\alpha_{obs} - \delta H\alpha_{coil}$, for the assigned residues of the domain 2 solubilized in 140 mM DPC (pH = 7, 313 K). The locations of the five helices observed in the crystallographic structure are shown in black, and the one-digit helix index obtained from chemical shifts is shown in grey. For the native helices, the transition residues at the helix endings were included in the helices.

contacts, all of which were assigned but one. The NOE intensities can be roughly classified in the order F61 > Y4 ≫ F3, which may be taken as reflecting side-chain relative mobility.

The aromatic NOE contacts observed for the sample in pure aqueous solution (data not shown) are quite similar to those observed for the the micellar solution, with only a few additional contacts for Y41, indicating a higher mobility for this side chain. However, in our experimental conditions, the sample in pure aqueous solution was found to contain an undesirable amount of peptide aggregates (see the next main section).

For the sample in micellar solution, the F61 side chain, however, presents interesting features since it shows a remarkable $i(i-1)$ NOE contact with γT57 in addition to the $i(i-1)$, $i(i+1)$, $i(i+3)$, and $i(i+4)$ contacts (Figure 6). The γT57-F61 contact is "native" in the sense that it should be observed in the native structure. Moreover, the δL65 protons exhibit, as the R62 α proton, a low-frequency shift that is *not observed* for the pure aqueous solution. These data could indicate the presence of a large and rather compact hydrophobic cluster centered on the F61 side chain and involving the residues T57, A64, L65, and the aliphatic part of the R62 side chain. This structure would be close to the native structure but *not identical*, given the chemical shift values for the α protons in the S55-D60 segment as previously mentioned.

Amide−Water Proton Exchange Analysis. At high temperature (above 313 K) the intensities of several correlations of the HSQC spectra recorded using water presaturation markedly decreased whereas others did not. To quantify these differences, HSQC experiments including field gradients were performed and the resulting spectra were compared to the standard spectra. For each labeled residue, Figure 7 represents the relative variation, in percent, of the HSQC cross-peak volumes recorded first using water presaturation and then using the gradient technique. The solvent−amide proton exchange of five residues—G14, L15, G16, D56, and G59—appears significantly faster. The first three residues are in the A−B loop, and the last two are in the transition region between the D and E helices.

Functional Analysis of Annexin I Domain 2 Solubilized in DPC Micelles. As mentioned above, the calcium site in the native structure involves the G14, L15, G16, and D56 residues, all ^{15}N-labeled in the annexin domain. To test the presence of this functional calcium site, HSQC spectra of the domain solubilized in DPC micelles were recorded after successive additions of calcium ions. However, even at high calcium concentration (180 mM), no significant variation in the HSQC spectrum was observed. Moreover, addition of short-chain phosphatidylserine lipids in the presence of calcium had no effect on the HSQC spectrum. These results show that, despite the stabilization of the secondary structure induced by the DPC micelles, the genuine calcium site of the annexin I domain 2 is not reconstituted in the isolated domain in the presence of large amounts of calcium and phosphatidylserine.

Relaxation Time Analysis. To further characterize the DPC/peptide complex, the ^{15}N transverse relaxation times (T_2) of the labeled amino acids were measured in the presence and absence of micelles, and, in parallel, the ^{31}P T_2 of the DPC head group was measured in the presence and absence of the domain. In aqueous solution, the ^{15}N T_2 values of the domain (between 95 and 180 ms) are in the same range as that obtained by Wagner et al. (1992) for the 70-residue Eglin protein (98−150 ms) under experimental conditions similar to ours. In the presence of 50 mM DPC, the ^{15}N T_2 values were found to be half as long (between 48 and 88 ms) with an average value corresponding to a 20−25 kDa protein. In the presence of the domain, the ^{31}P T_2 value of the DPC head group was also halved (320 and 160 ms in the absence and presence of the domain, respectively) and roughly corresponds to an overall correlation time of 10 ns, in agreement with the molecular size deduced from the ^{15}N T_2 values. These relaxation data strongly indicate that the DPC−peptide complex corresponds to one domain interacting with one DPC micelle as it is also demonstrated by the following CD and NMR experiments.

Titration of the Domain Secondary Structure by DPC

Because of the strong helix secondary structure enhancement induced by DPC micelles, a full titration of this effect was undertaken to get more information about the folding properties of the domain using circular dichroism and NMR spectroscopy.

CD Titration Curves. We recorded sets of CD spectra of the domain in the presence of increasing amounts of DPC micelles. Figure 10 shows the variation of the ellipticity at 222 nm versus DPC concentration. A plateau is clearly reached at a DPC/peptide ratio of about 50, which is very close to the DPC aggregation number, ∼55 (Lauterwein et al., 1979). These numbers demonstrate that the final peptide−micelle complex corresponds to one peptide molecule solubilized by one DPC micelle.

Presence of Peptide Aggregates. A set of twenty 2D ^{1}H−^{15}N HSQC spectra were recorded for DPC concentrations from 0.5 to 50 mM. From the first amounts of added DPC, most of the ^{1}H−^{15}N amide correlation peaks underwent measurable shifts in both frequencies. First, we noticed that at about 2 mM DPC (DPC/peptide = ∼1) the shifts were sufficient to allow the detection of several extra peaks approximately located at the frequencies of the peptide in the absence of DPC (Figure 8). The extra peaks were much less intense than the main signals with a 10/90 average volume ratio. Second, on increasing the DPC concentration,

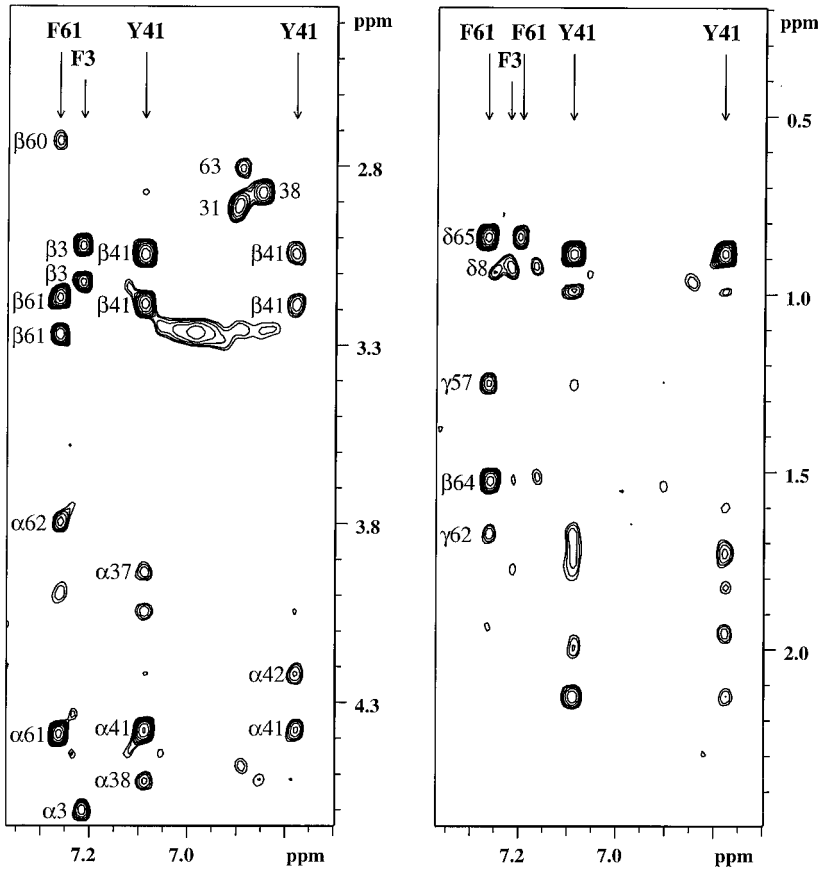

FIGURE 6: Aromatic region of the NMR NOESY spectrum of the domain 2 solubilized in 140 mM DPC (pH = 7, 313 K). Assigned NOE correlations are labeled with the residue numbers. The nonlabeled signals correspond to unassigned residues connected to Y41.

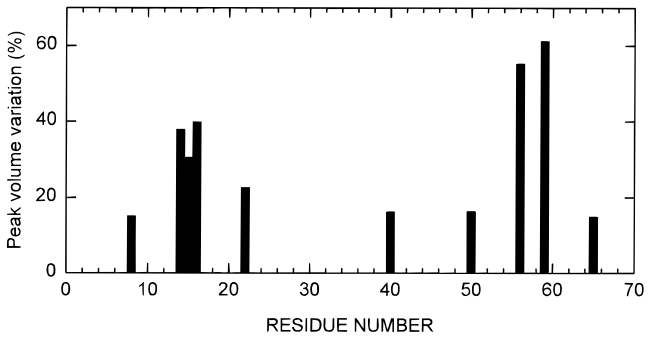

FIGURE 7: Relative variation, in percent, of the HSQC cross-peak volumes recorded using first water presaturation and then gradient pulses for the domain 2 solubilized in 120 mM DPC (pH = 6, 313 K).

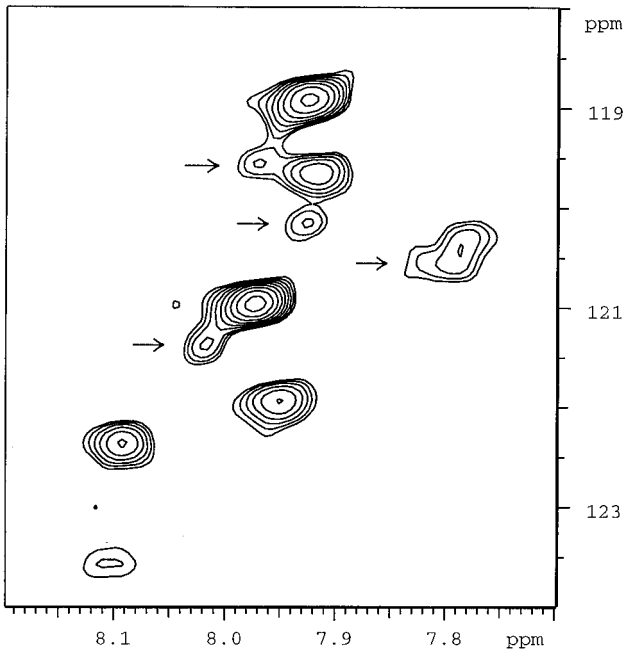

FIGURE 8: 500 MHz $^{1}H-^{15}N$ HSQC spectrum of annexin I domain 2 solubilized in 5 mM DPC (pH = 7, 303 K). A doubling of several signals is observed. Extra peaks are indicated with an arrow.

the location of the minor resonances was not significantly modified whereas the major components were further shifted. Lastly, above 15 mM DPC, the extra peaks were no longer detected. Such a phenomenon reveals the existence of what could be a slow exchange between two species, like those mentioned in several papers dealing with peptide and protein−DPC associations (McDonnell et al., 1993; van den Hooven et al., 1993). A possible explanation could be the presence of small amounts of oligomers or aggregates on which the effect of the DPC micelles significantly differs from that exerted on the monomer. We tested for the presence of aggregates by performing acrylamide gel electrophoresis under denaturing and non-denaturing conditions (Figure 9) for the domain solubilized in aqueous or in micellar solution. The purity of the sample is shown by a unique band in both denaturing gels. The wavy appearance of the band corresponding to the domain solubilized in micelles is an artifact due to the interaction of SDS with DPC. In contrast, the domain 2 gel in aqueous solution under non-denaturing conditions has two bands indicating the presence of aggregates. This is not the case for the domain solubilized in micelles.

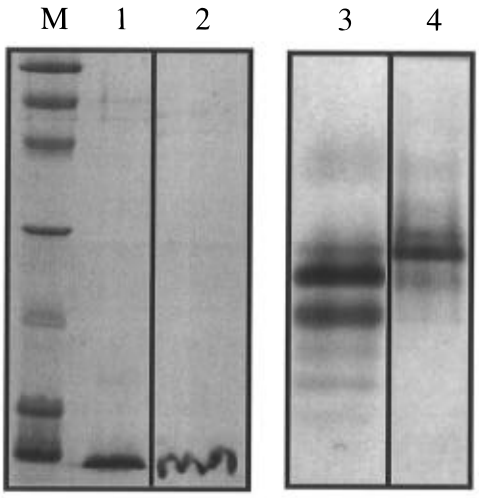

FIGURE 9: Left panel: Polyacrylamide gel electrophoresis under denaturing conditions (SDS) of the domain 2 samples. Lane M: molecular weight standards (top to bottom, 97.4, 66.2, 45, 31, 21, 14.4, and 6.5 kDa). Lane 1, aqueous solution sample. Lane 2, DPC solubilized sample. Right panel: Polyacrylamide gel electrophoresis under non-denaturing conditions of the domain 2 samples. For non-denaturing gels, the migration distance is not directly correlated with the molecular weight, thus molecular weight standards were not used. Lane 3, aqueous solution sample. Lane 4, DPC solubilized sample.

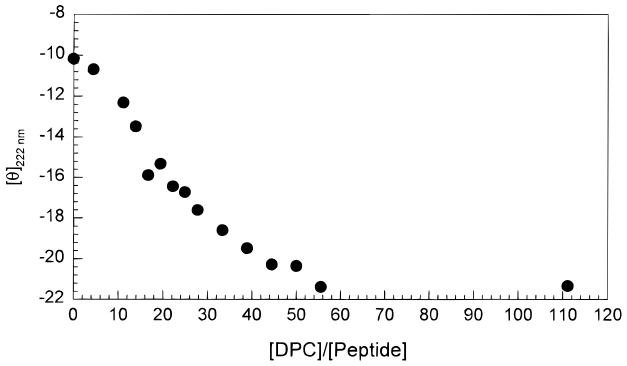

FIGURE 10: Variation of ellipticity with DPC concentration of the domain 2 (0.72 mM, pH = 7, 303 K).

Therefore, we suggest that low DPC concentrations are not able to solubilize the aggregates, as the exchange between aggregated and monomeric peptides is slow on the NMR time scale. At DPC concentrations above ~15 mM, the aggregates become solubilized and the corresponding signals become undetectable. The proportion of these aggregates is too small to affect the ^{15}N transverse relaxation rates measured for the domain in aqueous solution.

^{15}N NMR Titration Curves. The quantitative conformational interpretation of the ^{15}N chemical shift remains rather complex (Braun et al., 1994; Glushka et al., 1989; Le & Oldfield, 1994; Wishart et al., 1995; Wishart & Sykes, 1994). Nevertheless, the ^{15}N chemical shift variations, $\Delta\delta^{15}$N, are good indicators of the course of the structural change, within the different segments of the domain, associated with DPC titration. The ^{15}N chemical shift variation of the major correlation peaks are shown in Figure 11. The quantitative analysis of these titration data is rather complicated and is outside the scope of this work. The interesting result we want to point out is that the DPC concentration needed to reach the plateau also differs from one residue to another. For example, whereas G16 and A50 exhibit similar $\Delta\delta^{15}$N amplitudes, the slope at the origin of the G16 titration curve is significantly steeper than that relative to A50 (Figure 11). To get a crude estimate of these differences we simply measured a transition midpoint for each residue. For L8, G14, L15, G16, L22, and L65, the midpoint values were between 4 and 7 mM, whereas a value of 20 mM or more was found for V40 and A50. These data show that, during the titration, the conformational stabilization occurred earlier for the segments spanning the native A, B, and E helices than for the segments spanning the C and D helices and complement the circular dichroism data. The residues G14, L15, and G16, spanning the A−B loop, exactly follow the evolution of the residues within A and B helices, whereas residues D56 and G59 are virtually invariant (^{15}N *and* amide proton chemical shifts) during the titration.

The titration plots of Figure 11 exhibit a well-defined plateau region from about 50 mM DPC, i.e., from a DPC/peptide concentration ratio of about 50. Therefore, both CD and NMR data showed that at the end of the titration a steady state was reached for a molar protein to micelle ratio close to 1. This condition was achieved in several other published cases: myelin basic protein (Mendz et al., 1984, 1990), melitin (Lauterwein et al., 1979; Okada et al., 1994), cardiotoxin γ (Dauplais et al., 1995), and lantibiotic nisin (van den Hooven et al., 1993).

DISCUSSION

Domain 2 Does Not Constitute an Independent Folding Unit

Circular dichroism and NMR data clearly indicate that annexin I domain 2 is poorly folded in aqueous solution since only about one-fourth of the native helix content is detected. Therefore, the isolated domain 2 does not constitute an independent folding unit. However, the present experiments do not provide any indication of the compactness of the isolated domain although we may guess that this compactness is not very high, otherwise we would probably have observed a higher helix content. The apparent absence of folding cooperativity within the structural motif constituting the annexin building block is remarkable. This result has to be put in the context of present theories of protein folding (Dill et al., 1995; Fersht, 1995) as well as several recent experimental results (Creighton, 1995; de Prat Gay et al., 1995; Fink, 1995; Flanagan et al., 1992; Nishii et al., 1994; Peng & Kim, 1994) which tend to demonstrate that nonlocal interactions, acting in concert during the protein collapse, are the predominant interactions responsible for the full stabilization of secondary structures. Conversely, the residual helix content in the unfolded state of the domain in aqueous solution, ~25% as determined by circular dichroism, which is about 30% of native content, is far from being small as compared to what is observed for small proteins of the same size in the unfolded state (de Prat Gay et al., 1995) or even larger (Kippen et al., 1994a,b). The A and B helices account for most of this helix content, with probably a contribution from the E helix since this helix was proved to possess a reasonable propensity as compared to C and D helices as is discussed below. These results give some support to the idea that large multidomain proteins would need more extensive secondary structural framework in each domain than small single-domain proteins, of the same size range, to be folded in a reasonable time.

However it is important to recall that the full stability of the helix structures present in pure aqueous solution is not achieved. NMR clearly indicates, through chemical shift data, coupling constants, and number of NOE correlations, that the helix structures fluctuate around their equilibrium configuration, the A helix being slightly less fluctuating than the B helix, for example (Macquaire et al., 1993; Odaert et al., 1995). Existence of a TFE and micelle stabilizing effect on the isolated helix segments is of course clear evidence that these helices were not fully stabilized in pure aqueous solution and thus would be better qualified as *quasi-stable helices*.

Helix Propensities

Micelles have two expected effects: first to provide a large enough hydrophobic contact that could mimic intraprotein hydrophobic contacts and second, because their sizes are limited, to restrict the amplitude and frequency of overall spatial fluctuations of the different structural elements of the domain; in other words, to mimic some aspects of the initial collapse during the folding process. These effects have been observed for the A helix−loop−B helix domain subfragment (Macquaire et al., 1993).

The first question we wanted to address concerns the helical propensity for the different segments corresponding to the five helices. We know from the study of A helix−loop−B helix that the A and B segments have a high helical propensity in aqueous solution. For the remaining C, D, and E segments, data relative to $\Delta H\alpha$ in aqueous solution (Figure 2) are not fully reliable. This is because they concern a single residue per helix, and it is well-known that $\Delta H\alpha$ present characteristic oscillations for amphipathic helices, even though the large negative values of the $\Delta H\alpha$ for the segment E in micelles (Figure 5) would *per se* indicate a high helix propensity for this segment. Finally, a better answer comes from ^{15}N chemical shifts variation with DPC concentration. Clearly, the ^{15}N chemical shifts of the V40 (C helix) and A50 (D helix) residues reach a constant value only when the DPC/peptide ratio concentration is larger than 50, that is, when the protein−DPC complex is invariant with DPC concentration. On the other hand, residues in the A, B, and E segments reach their stabilized ^{15}N chemical shift values at a much lower, ∼20, DPC/peptide ratio. The hierarchy in the intrinsic helix propensity is thus A ∼ B ∼ E > C, D. Remarkably, the A, B, and E helices correspond to the interface between domain 2 and the remaining part of the protein (Figure 12) when C and D helices do not interact with the rest of the protein. The long-range interactions between domain 2 and the other domains can be clearly identified and are composed of (i) essentially hydrophobic interactions between B and E helices of both domains 2 and 3 making a sort of non-connected four-helix bundle and (ii) hydrophilic interactions made of salt bridges and hydrogen bond networks, located in the "central hydrophilic channel", between the A and B helices of domain 2 on one side and the A and B helices of domain 4 on the other side. Thus intrinsic helix propensities reflect the location of the segment within the native structure.

Structure of the Domain, Solubilized in Micellar Solution, in the Context of Protein Folding Process

The second range of questions concerns the existence of a compact state for the domain at DPC saturation and the

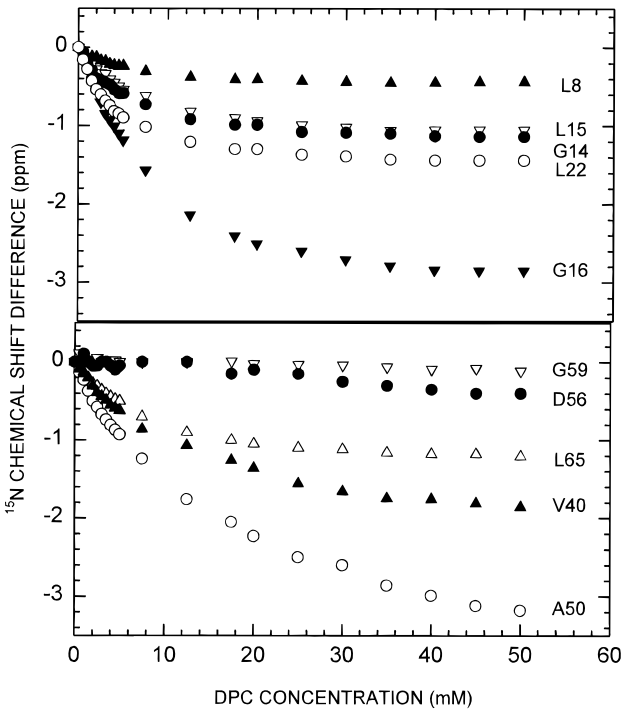

FIGURE 11: ^{15}N chemical shift of major correlation peaks of the HSQC spectra of annexin I domain 2 versus DPC concentration (pH = 7, 303 K).

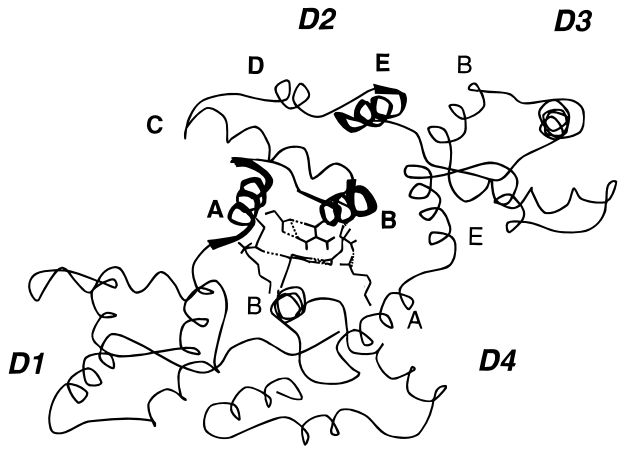

FIGURE 12: View of a wire trace of annexin I along the central axis. The A, B, and E helices of domain 2 are indicated by a wide ribbon, and their interfacial partners in domains 3 and 4 are indicated by a thin ribbon. The hydrogen-bonded side-chain networks locking the A, B, and E helices of domain 2 on one side and domains 2 and 3 on the other are also indicated in the hydrophilic central core of the protein.

importance and persistence of non-native residual structures. The presence of numerous local contacts between aromatic side chains and all neighboring side chains demonstrates that these aromatic side-chains are free to rotate around their $C\alpha-C\beta$ bonds, which rules out domain 2 being in a highly compact native-like state. However, side-chain NOE intensities are not all the same. Comparing NOE intensities for Y41 (C helix) and F61 (E helix) side chains indicates that the C helix is less stabilized than the E helix, which is in agreement with their propensities, and in addition a large hydrophobic cluster involving F61 is likely to occur with a long persistence time. This cluster formation may result in a stabilization of the clearly non-native conformation of the S55-G59 segment and particularly of the D56 residue. In the native protein, this residue is fully involved in the D

helix as the penultimate residue whereas the following residue, T57, is the transition residue between C and D helices. The remarkable positive value of the D56 ΔHα index and the quasi-absence of variation of its ^{15}N chemical shift with the DPC concentration indicate that this residue is persistently in a rather extended conformation. Remarkably, the D56 side chain is part of the calcium site found in domain 2. The non-native structure involving D56 may explain why calcium binding is not observed, although the A−B loop could adopt the suitable conformation for binding the ion. In the same context, high solvent accessibility was observed for the D56 residue and its neighbor G59 (Figure 7).

Lastly, the strong persistence in the A helix of the non-native capping box D_4ADE_7 is still observed in the domain and this rules out the formation of the major, native interhelix D4-R29 salt bridge locking the configuration of the A and B helices (Odaert et al., 1995). Therefore the observed A−B loop (G14, L15, G16) stabilization, or better the restriction of its dynamics, seems more likely to result from the freezing of the relative fluctuations of the two A and B helix cores, because of their interactions with the micelle, than from the formation of a local compact structure strictly due to a direct helix−helix interaction. Stabilization of the helix ends flanking the loop by simple capping, K13 and D18 for the A and B helices, respectively, may also contribute to the structuring effect on the loop.

Therefore, despite the large amount of helix secondary structure observed, we conclude that domain 2 does not adopt a rigid native-like structure in micelles. Whereas the role of micelles in increasing helix content and stability is clearly identified, it is not possible now to specify the degree of compactness that the domain has acquired in the micelle although we know that this compactness is not better than that observed for a "classical molten globule". Conversely we must say that we are unable to estimate to what extent micelles prevent the formation of a very compact structure once the secondary structure is formed. In our opinion, the structure observed for the isolated domain in micelle reflects the state of the same domain in the entire protein at a folding step where the collapse provides no more than *nonspecific* hydrophobic interactions between the different parts of the protein.

CONCLUSION

Our results can be summarized as follows: (i) the annexin domain is not an autonomous folding unit and is largely unfolded in pure aqueous solution, however (ii) it shows a significant amount of residual native helix structure as well as non-native structures; (iii) the residual structures are mainly located in the segments spanning the A, B, and probably E helices which present the highest helix propensity; (iv) the structure of these high-propensity segments is fully consolidated in a nonspecific hydrophobic environment, and the lower-propensity segment spanning the C and D helices is most probably not fully stabilized in the same environment; (v) high-propensity helices and quasi-stable helices of the domain in the unfolded state are those which have strong interactions with the other domains, and the low-propensity helices have only intradomain interactions; (vi) examination of the annexin crystallographic structure shows that the interactions between domains can be separated into two classes: one essentially hydrophobic interaction involving B and E helices in the intramodule interface D2-D3 (as well as D4-D1), and one essentially hydrophilic interaction between D2 and D4 involving the A helix−loop−B helix motif of both domains, which, remarkably, also concerns the residues involved in the non-native structure of the A helix.

In our opinion, the present observations concerning a specific hierarchy within helix propensities are important as far as they tend to demonstrate, at least for large, helix-containing, multidomain proteins, that, even if the formation of a compact folding intermediate (or "multicompact" intermediate) is a prerequisite to the *complete* stabilization of secondary helix structure, high helix propensity (most probably quasi-stable or even preformed helices) is necessary for the acquisition of a *global* compact structure capable of resuming the folding process. Because intrinsic helix propensities arise from local interactions between residues, such results obviously demonstrate that part of the information concerning the folding pathway is encoded in the protein sequence. In the case of annexin, the high propensity A helix−loop−B helix motif could, for instance, constitute an important framework, *during some yet undefined specific step* in the collapse, for the organization of the four domains around the symmetry axis passing through the hydrophilic core. In this respect it will be interesting to test, in the future, how the symmetry of the native structure is reflected, conserved or altered, in the helix propensities.

However, we still need a more precise description of structure propensities in the domain 2 as well as a better description of its average structure in pure aqueous solution and, importantly, of its compactness, that is, of the early state of folding of this domain. To this aim additional work is currently underway using a uniformly ^{15}N-labeled domain obtained by overexpression in *Escherichia coli* and synthetic subfragments spanning the C, D, and E helices.

SUPPORTING INFORMATION AVAILABLE

^{1}H chemical shifts of the assigned residues for the annexin I domain 2 solubilized in micellar solution at 318 K; ^{15}N and amide ^{1}H chemical shifts of the ten labeled residues for the annexin I domain 2 solubilized in micellar solution at 318 K (2 pages). Ordering information is given on any current masthead page.

REFERENCES

Baldwin, R. L. (1995) *J. Biomol. NMR 5*, 103−109.

Barton, G. J., Newman, R. H., Freemont, P. S., & Crumpton, M. J. (1991) *Eur. J. Biochem. 198*, 749−760.

Bewley, M. C., Boustead, C. M., Walker, J. H., Waller, D. A., & Huber, R. (1993) *Biochemistry 32*, 3923−3929.

Bollag, D. M., & Edelstein, S. J. (1995) *Protein Methods*, John Wiley & Sons, New York.

Braun, D., Wider, G., & Wuthrich, K. (1994) *J. Am. Chem. Soc. 116*, 8466−8469.

Chupin, V., Killian, J. A., Breg, J., de Jongh, H. H., Boelens, R., Kaptein, R., & de Kruijff, B. (1995) *Biochemistry 34*, 11617−11624.

Concha, N. O., Head, J. F., Kaetzel, M. A., Dedman, J. R., & Seaton, B. A. (1993) *Science 261*, 1321−1324.

Creighton, T. E. (1995) *Curr. Opin. Struct. Biol. 5*, 353−356.

Dauplais, M., Neumann, J. M., Pinkasfeld, S., Menez, A., & Roumestand, C. (1995) *Eur. J. Biochem. 230*, 213−220.

de Prat Gay, G., Ruiz Sanz, J., Neira, J. L., Itzhaki, L. S., & Fersht, A. R. (1995) *Proc. Natl. Acad. Sci. U.S.A. 92*, 3683−3686.

Dill, K. A., Bromberg, S., Yue, K., Fiebig, K. M., Yee, D. P., Thomas, P. D., & Chan, H. S. (1995) *Protein. Sci. 4*, 561−602.
Dobson, C. M. (1994) *Curr. Biol. 4*, 636−640.
Dobson, C. M., Evans, P. A., & Radford, S. E. (1994) *Trends Biochem. Sci. 19*, 31−37.
Fasman, G. D. (1995) *Biopolymers 37*, 339−362.
Favier-Perron, B., Lewit Bentley, A., & Russo-Marie, F. (1996) *Biochemistry 35*, 1740−1744.
Fersht, A. R. (1995) *Proc. Natl. Acad. Sci. U.S.A. 92*, 10869−10873.
Fink, A. L. (1995) *Annu. Rev. Biophys. Biomol. Struct. 24*, 495−522.
Flanagan, J. M., Kataoka, M., Shortle, D., & Engelman, D. M. (1992) *Proc. Natl. Acad. Sci. U.S.A. 89*, 748−752.
Glushka, J., Lee, M., Coffin, S., & Cowburn, D. (1989) *J. Am. Chem. Soc. 111*, 7716−22.
Gronenborn, A. M., Bax, A., Wingfield, P. T., & Clore, G. M. (1989) *FEBS Lett. 243*, 93−98.
Grzesiek, S., & Bax, A. (1993) *J. Am. Chem. Soc. 115*, 12593−12594.
Huber, R., Romisch, J., & Paques, E. P. (1990a) *EMBO J. 9*, 3867−3874.
Huber, R., Schneider, M., Mayr, I., Romisch, J., & Paques, E. P. (1990b) *FEBS Lett. 275*, 15−21.
Huber, R., Berendes, R., Burger, A., Schneider, M., Karshikov, A., Luecke, H., Romisch, J., & Paques, E. (1992) *J. Mol. Biol. 223*, 683−704.
Itzaki, L. S., Otzen, D. E., & Fersht, A. R. (1995) *J. Mol. Biol. 254*, 260−288.
Jimenez, M. A., Blanco, F. J., Rico, M., Santoro, J., Herranz, J., & Nieto, J. L. (1992) *Eur. J. Biochem. 207*, 39−49.
Jimenez, M. A., Munoz, V., Rico, M., & Serrano, L. (1994) *J. Mol. Biol. 242*, 487−496.
Kay, L. E., Torchia, D. A., & Bax, A. (1989) *Biochemistry 28*, 8972−8979.
Kippen, A. D., Arcus, V. L., & Fersht, A. R. (1994a) *Biochemistry 33*, 10013−10021.
Kippen, A. D., Sancho, J., & Fersht, A. R. (1994b) *Biochemistry 33*, 3778−3786.
Lauterwein, J., Bösch, C., Brown, L. R., & Wüthrich, K. (1979) *Biochim. Biophys. Acta 556*, 244−264.
Le, H., & Oldfield, E. (1994) *J. Biomol. NMR 4*, 341−348.
Lerner, L., & Bax, A. (1986) *J. Magn. Reson. 69*, 375−385.
Lewit Bentley, A., Bentley, G. A., Favier, B., L'Hermite, G., & Renouard, M. (1994) *FEBS Lett. 345*, 38−42.
Macquaire, F., Baleux, F., Huynh Dinh, T., Rouge, D., Neumann, J. M., & Sanson, A. (1993) *Biochemistry 32*, 7244−7254.
Markley, J. L. (1989) *Methods Enzymol. 176*, 12−89.
McDonnell, P. A., Shon, K., Kim, Y., & Opella, S. J. (1993) *J. Mol. Biol. 233*, 447−463.
Mendz, G. L., Moore, W. J., Brown, L. R., & Martenson, R. E. (1984) *Biochemistry 23*, 6041−6046.
Mendz, G. L., Brown, L. R., & Martenson, R. E. (1990) *Biochemistry 29*, 2304−2311.
Merrifield, R. B. (1963) *J. Am. Chem. Soc. 85*, 2149−2154.
Merutka, G., Dyson, H. J., & Wright, P. E. (1995) *J. Biomol. NMR 5*, 14−24.
Morgan, R. O., & Fernandez, M. P. (1995) *Mol. Biol. Evol. 12*, 967−979.
Moroder, L., Hallett, A., Keller, O., & Wersin, G. (1976) *Z. Physiol. Chem. 357*, 1651.
Moss, S. E. (1992) *The Annexins*, Portland Press Ltd, London, U.K.
Munoz, V., & Serrano, L. (1995) *J. Mol. Biol. 245*, 275−296.
Munoz, V., Serrano, L., Jimenez, M. A., & Rico, M. (1995) *J. Mol. Biol. 247*, 648-669.
Nishii, I., Kataoka, M., Tokunaga, F., & Goto, Y. (1994) *Biochemistry 33*, 4903−4909.
Odaert, B., Baleux, F., Huynh Dinh, T., Rouge, D., Neumann, J. M., & Sanson, A. (1995) *Biochemistry 34*, 12820−12829.
Okada, A., Wakamatsu, K., Miyazawa, T., & Higashijima, T. (1994) *Biochemistry 33*, 9438−9446.
Ortner, M. J., Sik, R. H., & Chignell, C. F. (1979) *Mol. Pharmacol. 15*, 179−188.
Papavoine, C. H., Konings, R. N., Hilbers, C. W., & van de Ven, F. J. (1994) *Biochemistry 33*, 12990−12997.
Peng, Z. Y., & Kim, P. S. (1994) *Biochemistry 33*, 2136−2141.
Pintar, A., Chollet, A., Bradshaw, C., Chaffotte, A., Cadieux, C., Rooman, M. J., Hallenga, K., Knowles, J., Goldberg, M., & Wodak, S. J. (1994) *Biochemistry 33*, 11158−11173.
Shaka, A. J., Barker, P. B., & Freeman, R. (1985) *J. Magn. Reson. 64*, 547−552.
Smith, L. J., Alexandrescu, A. T., Pitkeathly, M., & Dobson, C. M. (1994) *Structure 2*, 703−712.
Sopkova, J., Renouard, M., & Lewit Bentley, A. (1993) *J. Mol. Biol. 234*, 816−825.
Sopkova, J., Gallay, J., Vincent, M., Pancoska, P., & Lewit Bentley, A. (1994) *Biochemistry 33*, 4490−4499.
Stafford, R. E., Fanni, T., & Dennis, E. A. (1989) *Biochemistry 28*, 5113−5120.
Tam, J. P., & Heath, W. F. (1983) *J. Am. Chem. Soc. 105*, 6442−6447.
van den Hooven, H. W., Fogolari, F., Rollema, H. S., Konings, R. N., Hilbers, C. W., & van de Ven, F. J. (1993) *FEBS Lett. 319*, 189−194.
Wagner, G., Thanabal, V., Stockman, B. J., Peng, J. W., Nirmala, N. R., Hyberts, S. G., Goldberg, M. S., Detlefsen, D. J., Clubb, R. T., & Adler, M. (1992) *Biopolymers 32*, 381−390.
Weng, X., Luecke, H., Song, I. S., Kang, D. S., Kim, S. H., & Huber, R. (1993) *Protein Sci. 2*, 448−458.
Wishart, D. S., & Sykes, B. D. (1994) *Methods Enzymol 239*, 363−392.
Wishart, D. S., Sykes, B. D., & Richards, F. M. (1991a) *J. Mol. Biol. 222*, 311−333.
Wishart, D. S., Sykes, B. D., & Richards, F. M. (1991b) *FEBS Lett. 293*, 72−80.
Wishart, D. S., Sykes, B. D., & Richards, F. M. (1992) *Biochemistry 31*, 1647−1651.
Wishart, D. S., Bigam, C. G., Holm, A., Hodges, R. S., & Sykes, B. D. (1995) *J. Biomol. NMR 5*, 67−81.
Wu, L. C., Grandori, R., & Carey, J. (1994) *Protein Sci. 3*, 369−371.
Wüthrich, K. (1986) *NMR of Proteins and Nucleic Acids*, John Wiley & Sons, New York.
Yang, J. J., Buck, M., Pitkeathly, M., Kotick, M., Haynie, D. T., Dobson, C. D., & Radford, S. E. (1995) *J. Mol. Biol. 252*, 483−491.
Yang, J. T., Wu, C. S., & Martinez, H. N. (1986) *Methods Enzymol. 130*, 208−269.

BI960747V